ELSEVIER

Polymer 40 (1999) 857–870

polymer

Molecular deformation processes in aromatic high modulus polymer fibres

W.-Y. Yeh, R. J. Young*

Manchester Materials Science Centre, UMIST/University of Manchester, Grosvenor Street, Manchester M1 7HS, UK

Received 7 January 1998; accepted 26 March 1998

Abstract

Structure–property relationships in a number of different aromatic high-modulus fibres have been examined in detail. Fibres studied include Kevlar, Twaron, Technora and PBO and it has been shown using Raman spectroscopy that these fibres exhibit similar molecular deformation processes. The stress-induced shift of the 1610 cm^{-1} Raman band, assigned to a stretching mode of the *p*-phenylene ring, is found to be approximately -4.0 cm^{-1}/GPa for all of the fibres, independent of their chemical structures and morphologies. A similar rate of shift is found for the same band in poly(ethylene terephthalate) fibres. This implies that the molecular deformation processes in these different fibres are similar even though the fibres have different chemical structures and morphologies, and have been processed differently. It is shown that the mechanical behaviour of the fibres is consistent with deformation following a uniform stress series aggregate model.

Keywords: Ppoly(*p*-phenylene terephthalamide); Copoly(*p*-phenylene/3, 4′ oxydi-phenylene terephthalamide); Poly(*p*-phenylene benzobisoxazole)

1. Introduction

Significant advances have been made in the development of high-performance fibres over the past 30 years and remarkable progress has been made in the production of so-called ultra-high modulus fibres. The 1980s saw the development of high-modulus polyethylene fibres [1]. Other examples include poly(*p*-phenylene terephthalamide) (PPTA), poly(*p*-phenylene benzobisthiazole) (PBT), poly (*p*-phenylene benzobisoxazole) (PBO), poly(*p*-benzamide) (PBA) etc. [2]. These high-performance fibres not only have high tensile strength and modulus but also have other impressive properties such as good dimensional stability, thermal and chemical resistance [2].

The increasing use of such organic fibres in industrial applications has led to the need for a better understanding of the mechanisms of deformation in the materials. Raman spectroscopy has been applied successfully to study molecular deformation process for a wide variety of high-performance polymer fibres [3]. The shift to lower wavenumber of the Raman band at 1610 cm^{-1} for Kevlar 49, assigned to stretching of the *p*-phenylene ring, was found to be approximately -5.0 cm^{-1}/% [4]. Such strain-induced shifts have been found to be somewhat smaller in lower-modulus, less-oriented Twaron aramid fibres since in this case the polymer chains experience less stress because of the differences in morphology [5]. The detailed molecular deformation processes for high-performance rigid-rod polymer fibres such as PBT and PBO have also been investigated using Raman spectroscopy by Young and co-workers [6,7].

The purpose of this present investigation is to study the relationship between the structure and mechanical properties of a variety of aramid and PBO fibres. Molecular deformation processes were studied for the fibres subjected to axial deformation using Raman spectroscopy. In each case the Raman band at about 1610 cm^{-1}, due to a symmetrical vibration mode of the *p*-phenylene ring, was used to follow the deformation behaviour because this band is intense and well-defined for all of these fibres. The deformation micromechanics for these fibres are then compared with the behaviour of conventional poly(ethylene terephthalate) (PET) fibres.

2. Experimental

2.1. Materials

A range of different aramid fibres were used in this work including several grades of Kevlar® and Twaron® fibres. Details of the suppliers, fibre types and diameters of the monofilaments are listed in Table 1. The aramid fibres are based upon the poly(*p*-phenylene terephthalamide)

* Corresponding author.

0032-3861/98/$ - see front matter
PII S0032-3861(98)00308-5

Table 1
Aramid and PBO fibres used in this work

Fibre	Supplier	Type	Appearance	Diameter (μm)
Kevlar 29	Du Pont	Commercial	Yellow	11.3
Kevlar 49	Du Pont	Commercial	Yellow	12.0
Kevlar 149	Du Pont	Commercial	Yellow	12.0
Twaron IM	Akzo Nobel	Experimental	Yellow	12.5
Twaron IM	Akzo Nobel	Experimental	Yellow	12.6
Twaron HM	Akzo Nobel	Experimental	Yellow	11.8
Technora	Teijin	Commercial	Gold	13.2
PBO	Toyobo	Experimental	Gold	12.5

molecule [2] with the following repeat unit:

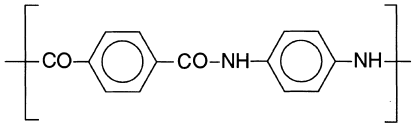

The tensile and compressive properties of the Kevlar and Twaron aramid fibres have been studied in detail by Andrews and Young [8]. The fibres were produced in a systematic way to have different properties, however, the details of the processing conditions are confidential to the manufacturers.

The Technora® and PBO fibres were supplied by Teijin Ltd, Japan, and Toyobo Ltd, Japan, respectively. Technora is an aramid copolymer with a copoly(*p*-phenylene/3, 4′ oxydi-phenylene terephthalamide) repeat unit thought to be of the form [2]:

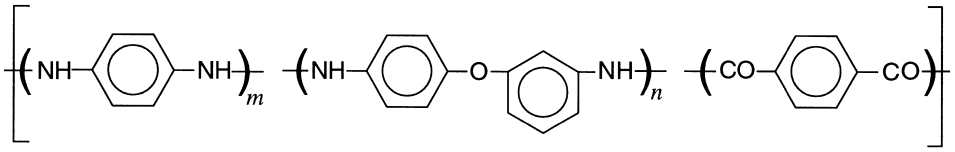

where m and n are mole fractions such that $m + n = 1$. It is thought [2] that $m \approx n \approx 0.5$ in commercial Technora fibre. PBO fibres have recently been given the trade name Zylon® and contain poly(*p*-phenylene benzobisoxazole) molecules with the following repeat unit:

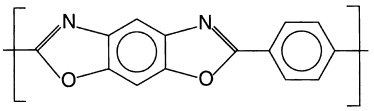

Some physical properties of typical Technora and PBO fibres reported by Teijin Ltd and Toyobo Ltd, respectively, are given in Table 2.

Table 2
Physical properties of Technora and PBO fibres (manufacturer's data)

Physical properties	Technora fibre	PBO fibre
Density	1.39 g/cm^3	1.56 g/cm^3
Tensile strength	3.4 GPa	5.5 GPa
Tensile modulus	73 GPa	280 GPa
Elongation at break	4.6%	2.5%
Decomposition temperature	500°C	650°C
Moisture regain	2.0%	0.6%

2.2. Wide-angle X-ray scattering (WAXS)

Flat-plate X-ray diffraction analysis was performed using Phillips PW1020 flat plate diffractometer operated at 40 kV and 30 mA. Yarns of the Kevlar, Twaron, Technora and PBO fibres were aligned unidirectionally in the holder and then irradiated with Ni-filtered CuKα radiation for a minimum time of 30 min. The resultant patterns were collected on X-ray sensitive photographic film using a specimen-to-film distance of 50 mm.

Samples of the fibres were also prepared by mounting yarns parallel to each other on the glass slides which were then placed in the holder of a Phillips PW1800 powder diffractometer operated at 40 kV and 50 mA. They were then irradiated with Ni-filtered CuKα radiation (wavelength = 0.154 nm). Equatorial scans were obtained and analysed between 2θ Bragg angles of 5° and 60° using a step size of 0.02° at a scan rate of 1.2°/min. The data were collected on a PC computer attached to the diffractometer.

2.3. Mechanical testing

Monofilaments of the Kevlar, Twaron, Technora and PBO fibres were mounted across a cardboard window using Ciba-Geigy HY/LY 1927 two-parts cold-curing epoxy resin. A minimum of 48 h was allowed for the adhesive to set completely at 23°C prior to testing to minimize slippage errors. All specimens were tested using an Instron 1121 universal testing machine following the recommendations given in ASTM D3379-75. A Macintosh II computer was connected to the tensile tester and the software 'Workbench 3.1' was used to read the load–time data, which was then converted into stress–strain curves. A sampling rate of 100 ms, i.e. 10 points per second, was used to collect the

data. The fibre-mounted window with a pre-determined gauge length of 50 mm was placed within the grips of the tensile tester and the two ends separated after carefully cutting both sides of the cardboard window.

Fibre specimens were tested at a constant rate of $1.67 \times 10^{-3}\,s^{-1}$ using cross-head speed of 5 mm/min. A full scale load of 1 N was found to be adequate for these specimens and a standard weight of 1 N was used to calibrate the Instron tester. A minimum of 20 specimens were tested for each type of fibre and the testing conditions were controlled to be 23 ± 1°C and 50 ± 5% relatively humidity.

2.4. Raman spectroscopy

A Renishaw 1000 Raman Imaging Microscope was used to record the full Raman spectra of the fibres. A low power of 25 mW He–Ne laser (632.8 nm) was employed with an intensity of about 1 mW when focused on the monofilaments. The laser spot diameter was about 2 μm. The 180° back scattered light was collected by the microscope objective (× 50) and then analysed using a grating system. A highly-sensitive Peltier-cooled charge-coupled device (CCD) detector, was used to record the spectra. The Renishaw software with a PC computer was used to control the whole system, display spectra in graphical form and process the data.

Raman spectra of the different fibres were obtained during deformation using the 632.8 nm red line of a 15 mW He–Ne laser with an intensity of about 1.0 mW at the fibre. The low-power laser spot was focused in an Olympus microscope to a spot about 2 μm diameter on the fibre. The 180° back scattered light was collected by the microscope objective (×50) and then analysed using a Spex 1000 single monochromator. A highly-sensitive CCD camera, cooled with liquid nitrogen, was used to record the spectra. The CCD camera was linked by an interface to a computer system where Wright Instruments AT1 software was used to control the camera readout operation, display spectra in a graphical form and process the data.

It was found that Lorentzian curve fitting could be used to analyse all of the Raman spectra. Both the undeformed and deformed Raman spectra for the fibres were generally symmetric in shape and could be fitted quite well to the Lorentzian function, $L(x)$;

$$L(x) = \frac{I \times W^2}{[(x-P)^2 + W^2]} \tag{1}$$

where P is the band position, W is the full width at half maximum intensity, and I represents the intensity of Raman scattering. The 'goodness of fit' can be measured from a chi-squared parameter, χ^2 [9], a measure of the difference between the fitted curve and the raw Raman data given by:

$$\chi^2 = \frac{\Sigma(I_R - I)}{n} \tag{2}$$

where I_R is the intensity of the Raman data and n is the number of data points. During the curve-fitting procedure the program continuously adjusts the fitting parameters in order to minimize the chi-squared value. As well as the band position, other valuable information which can be obtained from the spectra is the full width at half maximum (FWHM) which provides information about molecular stress distributions. Also, a convenient way of quantifying the degree of asymmetry of a Raman band is the asymmetry ratio, where *SI* is the symmetry index [10]. A combination of these parameters will be utilized to describe the structure of the fibres and the molecular deformation processes induced by the macroscopic stress.

2.5. Molecular deformation by straining and stressing

Raman spectra were obtained from individual monofilaments during deformation at 23 ± 1°C. All fibres were fixed on a straining rig using aluminium foil tabs and cyanoacrylate adhesive to give a gauge length of 50 mm. The axes of the fibres were aligned to be parallel to the polarization direction of the incident laser beam to within ± 5°.

For straining experiments, the monofilaments were stretched to failure in steps of the order of 0.2% strain. The displacement was applied in a staircase fashion. Each incremental deformation step required 60 s with 30 s to focus the beam on the fibre before exposure. Hence an effective strain-rate of $3.33 \times 10^{-5}\,s^{-1}$ was used in stretching the fibres.

For stressing experiments, the monofilaments were deformed by adding weights of the order of 2 g (at $\sim 2 \times 10^{-2}$ N/min) to a scale pan connected to the fibre over a pulley for the Kevlar, Twaron and Technora fibres, and 5 g (at $\sim 5 \times 10^{-2}$ N/min) for the PBO fibres. The diameter of all individual fibres was measured to within ~0.1 μm before deformation in an optical microscope using an Image Analyser system.

3. Results and discussion

3.1. WAXS analysis

The flat-plate WAXS patterns obtained from the yarns of Kevlar 49 and Twaron IM fibres are shown in Fig. 1. It can be seen from the narrow spread of the arcs for the Kevlar 49 fibre in Fig. 1*a* that there is a high degree of molecular orientation along the fibre axis. A similar flat-plate WAXS pattern was also observed for the Twaron IM fibre (Fig. 1*b*) again showing a high level of molecular orientation along the fibre axis. Fig. 2*a* and *b* shows WAXS diffractometer equatorial traces for Kevlar 49 and Twaron IM fibres, respectively. There are two well-defined crystalline peaks observed corresponding to Bragg reflections from the (110) and (200) crystal planes of the orthorhombic unit cell [11–13]. The values of the *d*-spacings of the (110) and (200)

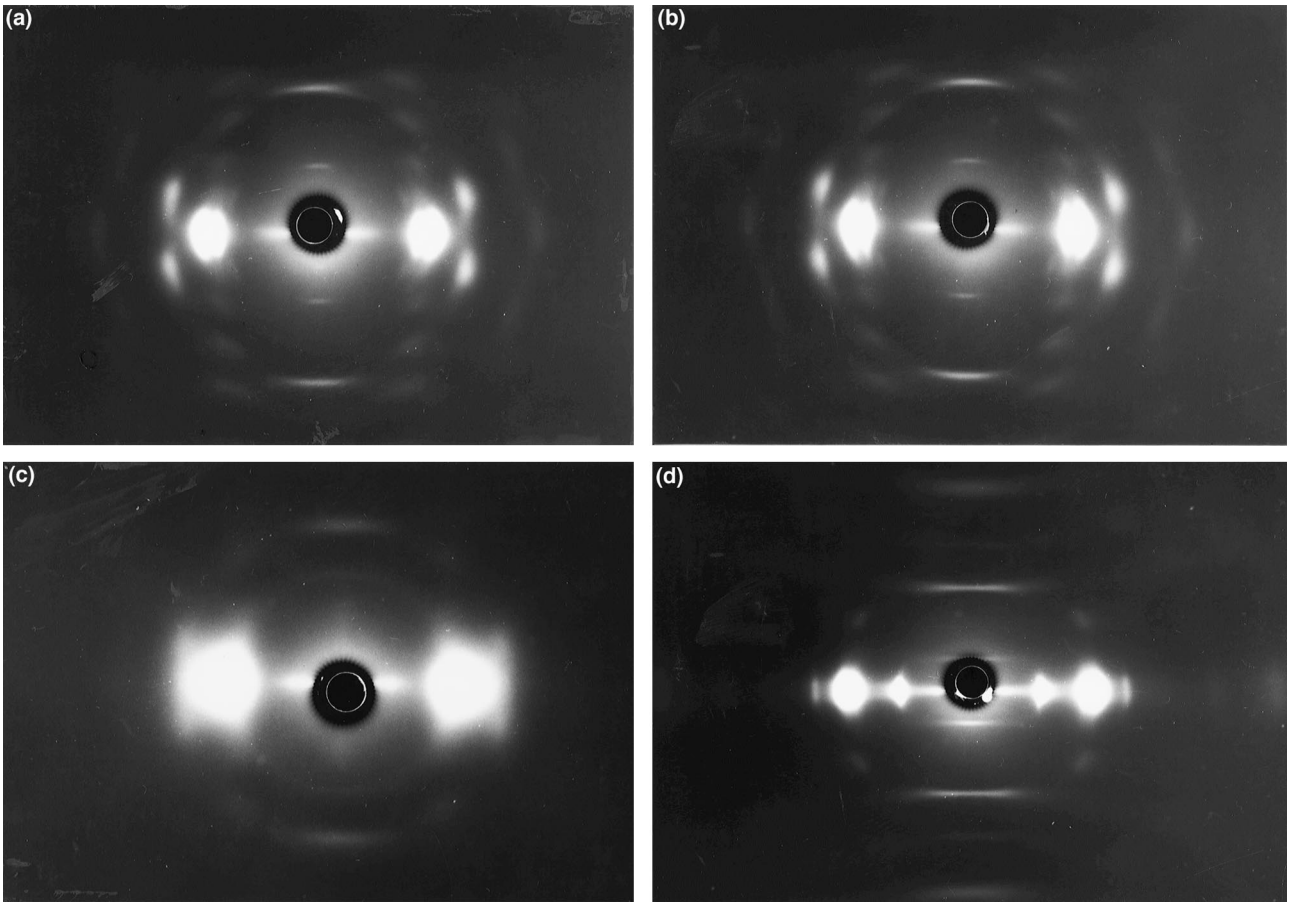

Fig. 1. Flat-plate WAXS patterns of (a) Kevlar 49, (b) Twaron IM, (c) Technora, (d) PBO fibres.

reflections are 0.430 and 0.386 nm for the Kevlar 49 fibre and 0.429 and 0.383 nm (all $\pm$ 0.005 nm) for the Twaron IM fibre, which are consistent with the literature values.

The flat-plate WAXS patterns obtained from yarns of the Technora and PBO fibres are shown in Fig. 1*c* and *d*, respectively. It can be seen from the arcing in the patterns that both fibres show a high degree of axial molecular orientation along the fibre axes. The molecular packing and ordering of the Technora fibre is potentially complex because of the completely random monomer sequence. Blackwell *et al.* [14,15] studied the chain conformations of similar Technora copolyamide fibres. They found a similar WAXS pattern which consisted of a series of non-periodic layer lines with the meridional peak positions predicted accurately for a fully-extended chain conformation.

The WAXS pattern for the PBO fibres in Fig. 1*d* consists of sharp equatorial peaks, non-periodic layer lines and off-axis, first order (*hkl*) reflections which indicates that there is a level of three-dimensional crystallinity in the heat-treated fibres [16,17]. The three-dimensional crystallinity in PBO is due to its planar molecules which improve chain-axis registry. However, only first-order (*hkl*) reflections are present in PBO, whereas a number of higher-order (*hkl*) reflections are observed in Kevlar and Twaron fibres, indicating that the PBO crystalline structure is not as well-ordered as in the Kevlar and Twaron fibres.

Typical equatorial diffractometer traces obtained from WAXS analysis of the as-received Technora and PBO fibres are shown in Fig. 2*c* and *d*, respectively. It can be seen that a single-intensity maximum occurs for the Technora fibres at $2\theta = 20.1°$. The crystalline peaks of the PBO fibres occur at $2\theta = 16.2°$, 27.5° and 32.7° which correspond to *d*-spacing in the crystal structure of 0.547, 0.324 and 0.274 nm (all $\pm$ 0.005 nm). From the above results, it can be concluded that the Technora fibre has a structure consisting of a fully-extended chain conformation along the fibre axis with poorly-defined transverse packing. The PBO fibre, however, shows a high degree of axial orientation of the molecules along the fibre axis with better transverse packing of the molecules.

3.2. Mechanical testing

Fig. 3*a* and Fig. 4*a* show the stress–strain curves for all the Kevlar and Twaron aramid fibres. Their tensile properties are summarized in Table 3 and it can be seen that for both sets of fibres the increase in the fibre modulus is accompanied by a significant reduction in tensile strength. Fig. 3*b* and Fig. 4*b* show the modulus–strain curves of these fibres. The tensile modulus increases with strain for all the

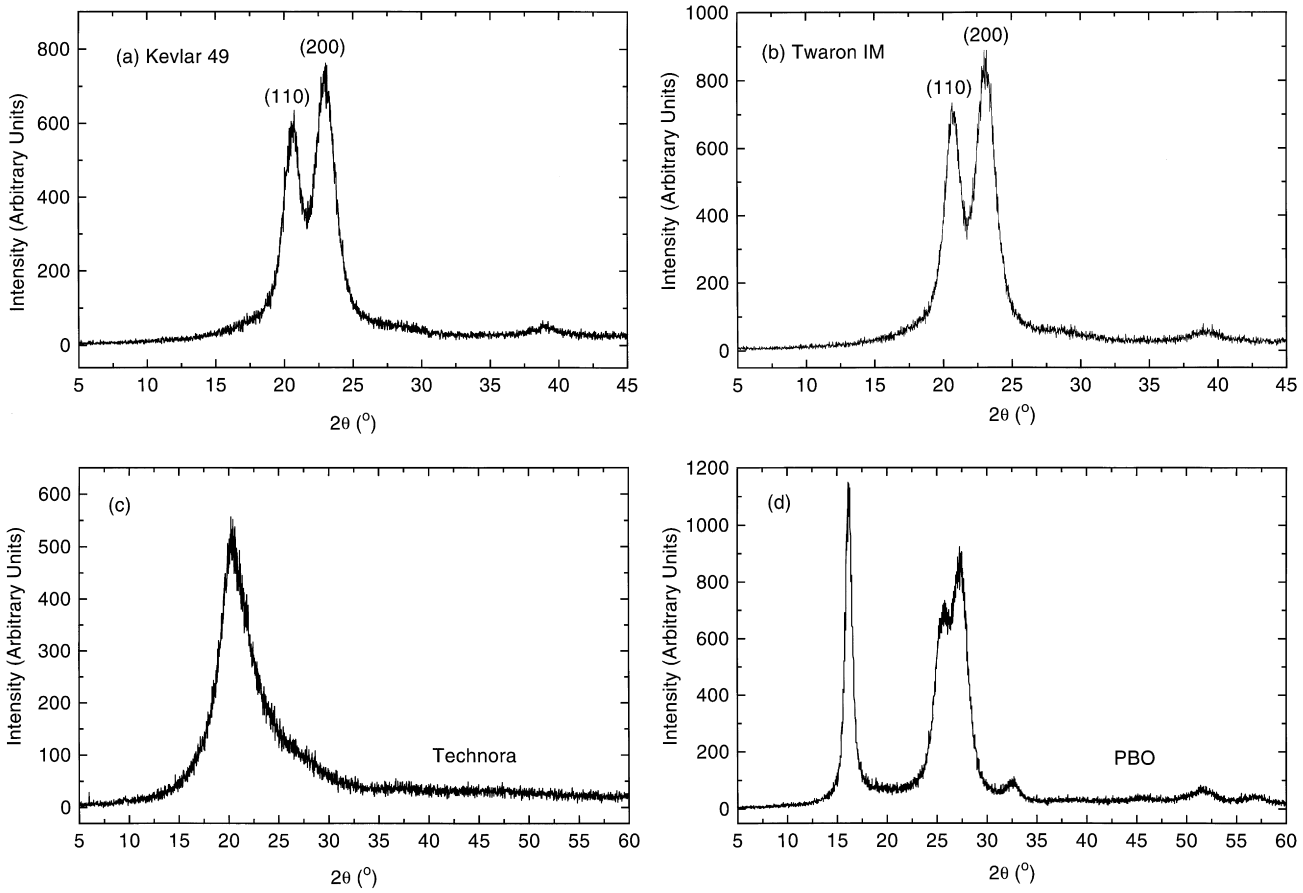

Fig. 2. WAXS diffractometer traces of (a) Kevlar 49, (b) Twaron IM, (c) Technora, (d) PBO fibres.

aramid fibres due to an increase in molecular alignment along the fibre axis during tensile deformation [18–20].

Typical stress–strain curves and their first derivatives are shown in Figs 5 and 6 for the Technora and PBO fibres. It can be seen that the stress–strain curves of both fibres are approximately linear up to fracture with no indication of yielding. Similar behaviour for PBO fibres was found by Young *et al.* [7] and Ang [17]. The modulus–strain curves for the Technora and PBO monofilaments have characteristic shapes with the modulus showing two and one maxima, respectively. For the Technora fibres the modulus at the first maximum is at approximately 76 GPa (0.3% strain) and with the second maximum at approximately 82 GPa (2.6% strain) as shown in Fig. 5. From Fig. 6, it can be seen that the maximum modulus for PBO is at approximately 225 GPa (0.9% strain). The tensile properties of Technora and PBO fibres determined using a gauge length of 50 mm are listed in Table 3 with the modulus being measured in this case from the initial slope of the stress–strain curve.

The tensile properties of Kevlar and Twaron fibres are in good agreement with the results reported by Andrews and Young [8] and those for Technora and PBO fibres are close to the reported data of the suppliers, except for the tensile modulus of the PBO fibre (Table 2). The reported value of 280 GPa [21] is significantly higher than the measured value of 192 GPa obtained using a 50 mm gauge length. It is well established that the determination of modulus of high-modulus polymer fibre is particularly sensitive to the end effects [17] and the fibre modulus will be reduced for a finite gauge length. The supplier's value had been measured upon twisted PBO yarn with the diameter being determined from the fibre denier and density [21]. In this present study the fibre diameters were measured directly using SEM. It is well established that PBO fibres contain a significant number of capillary voids [21]. Hence, direct measurements of fibre diameter will lead to lower values of modulus being determined than when the fibre denier is employed. It appears therefore that the discrepancy in PBO modulus can be explained as a combination of end effects and voiding in the fibres.

3.3. Raman spectroscopy

Fig. 7*a* and *b* shows the Raman spectra obtained in the range 600–1800 cm^{-1} for a Kevlar 49 fibre and a Twaron IM fibre, respectively. There are over 10 well-defined Raman-active bands in this region that have been assigned by Kim *et al.* [22]. No significant difference was observed between the Raman spectra of any of the Kevlar and Twaron fibres even though they have different mechanical properties. Young *et al.* [4,23–26] have reported that most of the Raman bands in the region 1100 and 1700 cm^{-1} shift to

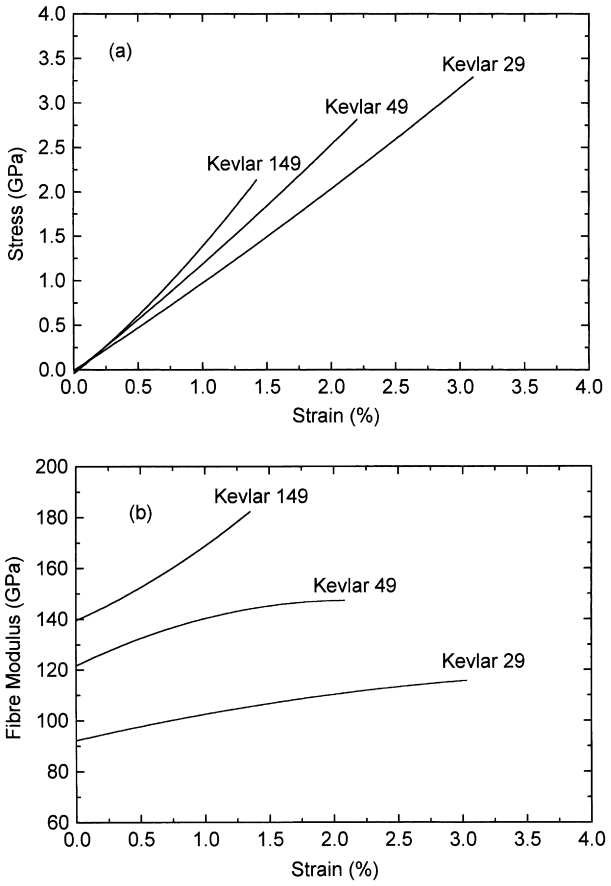

Fig. 3. (a) Stress–strain curves of the Kevlar fibres. (b) Modulus–strain curves of the Kevlar fibres.

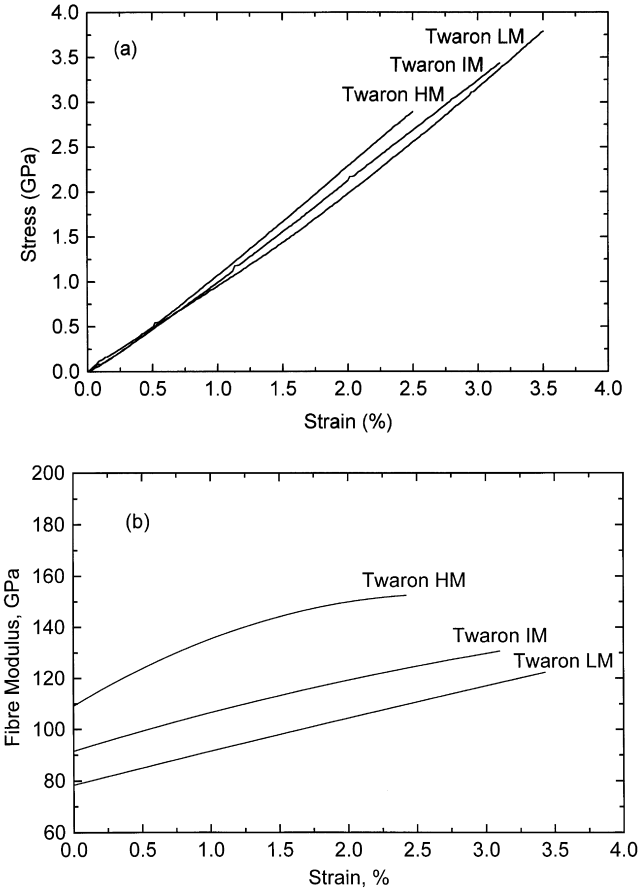

Fig. 4. (a) Stress–strain curves of the Twaron fibres. (b) Modulus–strain curves of the Twaron fibres.

lower wavenumber upon the application of a tensile strain due to changes in bond length and force constants [3]. This present study is confined to monitoring the deformation of aramid fibres using the Raman band at around 1610 cm^{-1} which has been assigned to the vibrational mode 8a of the *p*-phenylene ring [22,27]. This band is present in all the aromatic polymer fibres studied and the exact positions of the band for the aramid fibres (before deformation) are listed in Table 4.

Fig. 7*c* and *d* show the full Raman spectra obtained in the range 600–1800 cm^{-1} for a Technora fibre and a PBO fibre, respectively. A strong fluorescence background was observed in both spectra due probably to some degradation of the fibres during processing [17]. The spectrum of Technora fibres is quite complex, presumably due to it being a copolymer. There are over 10 Raman-active bands in this range (Fig. 7*c*). As far as the authors are aware, the Raman spectrum has not been reported previously for Technora fibres, neither have assignments of the Raman bands been made. Nevertheless there is a well-defined Raman band at 1614 cm^{-1} that is almost certainly related to the symmetric vibrational mode of the *p*-phenylene ring [22,27].

It can be seen in Fig. 7*d* that there are at least six principal well-defined bands found in the Raman spectrum of the PBO fibre. It has not been possible to assign them to molecular vibrations due to the lack of theoretical Raman analyses, but it is likely that the strong band at around 1620 cm^{-1} can also be assigned to the symmetric vibrational mode of the *p*-phenylene ring. Young *et al.* [7] and Ang [17] found that for heat-treated PBO fibres, the peak positions of the three bands at 1280, 1540 and 1615 cm^{-1} were all sensitive to the level of tensile strain.

The difference in exact position of the Raman band for the different types of fibres shown in Table 4 may be due

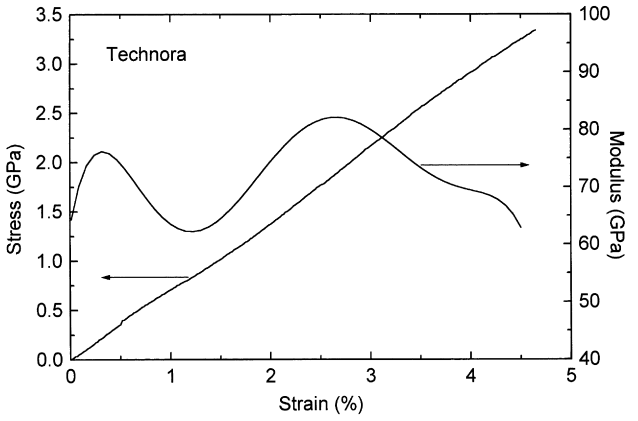

Fig. 5. Stress–strain curve and modulus–strain curve for a Technora fibre.

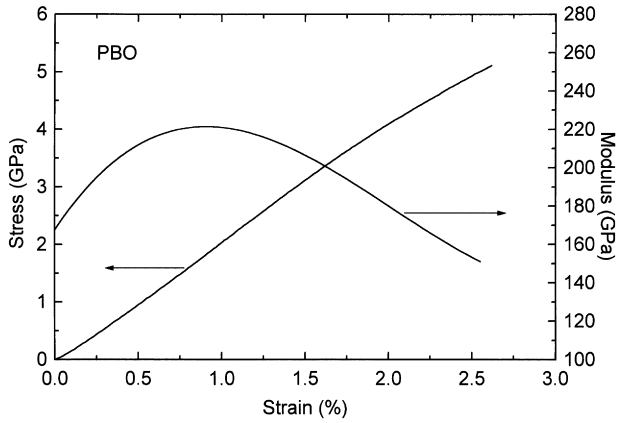

Fig. 6. Stress–strain curve and modulus–strain curve for a PBO fibre.

to differences in chemical environment around the *p*-phenylene ring and the microstructure of the fibres [9].

3.4. Molecular deformation by straining and stressing

The 1610 cm^{-1} Raman bands for Kevlar and Twaron fibres shift to lower wavenumber and broaden upon the application of a tensile stress, as shown in Fig. 8*a* and *b*. Unlike recent observations for PET fibres [28], the Raman bands for these aramid fibres have a symmetric shape both before and after deformation, i.e. *SI* values [10] equal to 1. Hence, the Lorentzian curve fitting can be used to analyse all of the Raman spectra. The dependence of the 1610 cm^{-1} Raman band peak positions upon strain for the Kevlar and

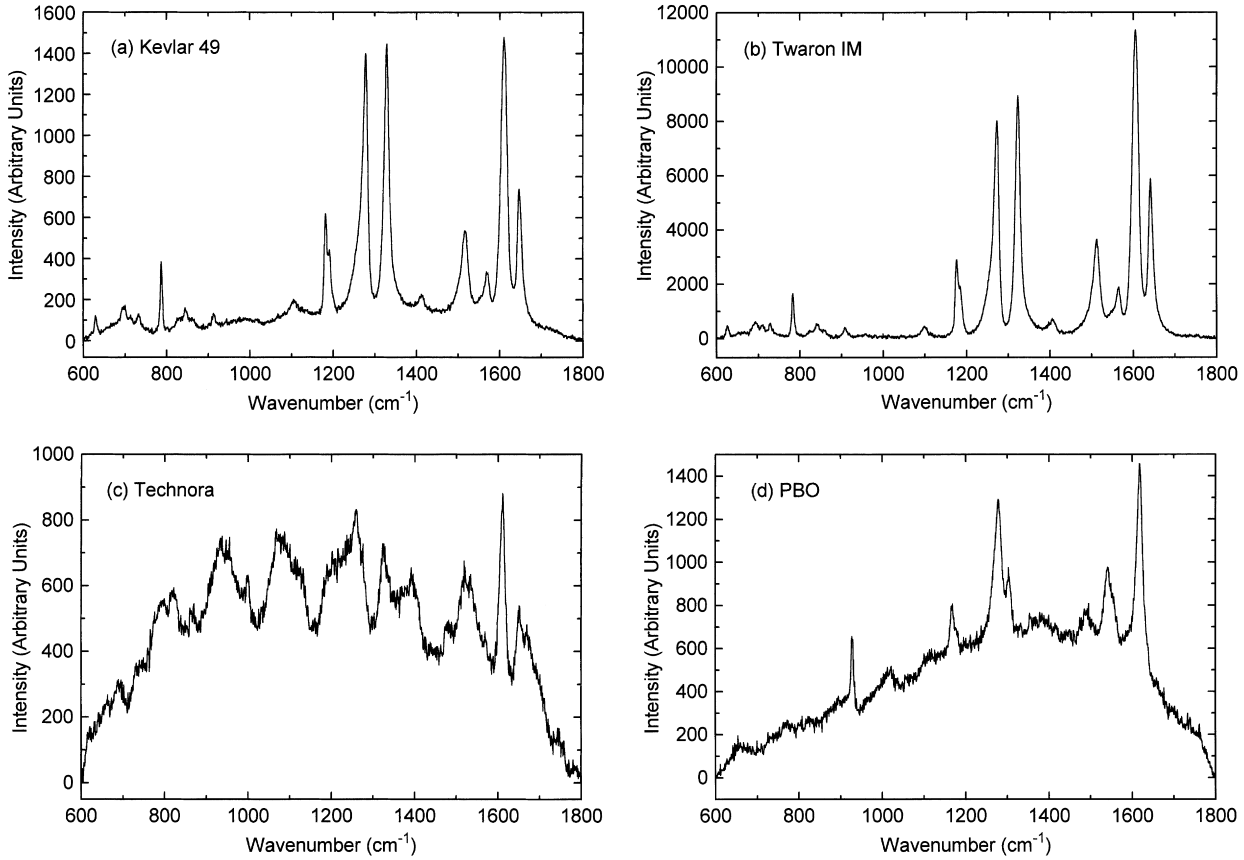

Fig. 7. Full Raman spectra for the monofilaments of (a) KevIar 49, (b) Twaron IM, (c) Technora, (d) PBO fibres obtained with the fibre axes parallel to the direction of po1arisation of the laser beam.

Table 3
Tensile properties of Kevlar, Twaron, Technora and PBO fibres (gauge length ~50 mm)

Fibre	Young's modulus (GPa)	UTS (GPa)	Failure strain (%)
Kevlar 29	93 ± 11	3.3 ± 0.6	3.1 ± 0.4
Kevlar 49	123 ± 8	2.8 ± 0.5	2.2 ± 0.4
Kevlar 149	141 ± 6	2.1 ± 0.3	1.4 ± 0.3
Twaron LM	78 ± 5	3.6 ± 0.4	3.5 ± 0.4
Twaron IM	93 ± 6	3.4 ± 0.3	3.2 ± 0.4
Twaron HM	108 ± 8	2.9 ± 0.4	2.5 ± 0.3
Technora	73 ± 4	3.3 ± 0.2	4.7 ± 0.2
PBO	192 ± 10	5.2 ± 0.3	2.7 ± 0.2

Table 4
Values of Raman band shift due to strain and stress for the aramid and PBO fibres

Fibre	Undeformed band position (cm^{-1})	Strain-induced Raman band shift (cm^{-1}/%)	Stress-induced Raman band shift (cm^{-1}/GPa)	Stress-induced Raman band broadening (cm^{-1}/GPa)
Kevlar 29	1610	− 3.2 ± 0.3	− 3.9 ± 0.2	3.4 ± 0.3
Keylar 49	1610	− 4.5 ± 0.3	− 3.9 ± 0.2	2.8 ± 0.2
Keylar 149	1610	− 5.1 ± 0.4	− 4.0 ± 0.3	1.1 ± 0.1
Twaron LM	1610	− 3.2 ± 0.2	− 3.9 ± 0.2	3.4 ± 0.3
Twaron IM	1610	− 3.5 ± 0.2	− 4.0 ± 0.2	3.5 ± 0.2
Twaron HM	1610	− 3.7 ± 0.3	− 4.0 ± 0.4	2.5 ± 0.2
Technora	1614	− 2.9 ± 0.3	− 4.0 ± 0.4	6.8 ± 0.4
PBO	1621	− 8.1 ± 0.4	− 3.9 ± 0.2	2.1 ± 0.2

Twaron fibres are shown in Fig. 9*a* and *b*, respectively. The shift of the Raman band with strain is approximately linear up to fracture for these aramid fibres and tends to increase with increasing fibre modulus, which is in agreement with the observations of Andrews *et al*. [24–26]. The dependence of the positions of the 1610 cm^{-1} Raman band upon stress for the Kevlar and Twaron fibres is shown in Fig. 10*a* and *b*, respectively. It is found that not only is the peak shift of the Raman band proportional to stress but, most significantly that data for the different fibres all fall on the lines of identical slope (approximately − 4.0 cm^{-1}/GPa).

A significant increase of FWHM was observed during tensile deformation of the Kevlar and Twaron fibres, as shown in Fig. 11*a* and *b*. The increase of FWHM with stress is approximately linear up to fracture for these aramid fibres and the values of the stress-induced band broadening factors are listed in Table 4. It can be seen in Fig. 12 that the stress-induced band broadening factor decreases with increasing fibre modulus with Kevlar 149 having the lowest value (about 1.1 cm^{-1}/GPa). This is due to the higher level of molecular orientation in Kevlar 149 fibre which results in a more even load distribution on molecules within the fibres during tensile deformation. Fig. 12 shows the dependence of the stress-induced band broadening upon fibre modulus. It can be see that a straight line fitted to the data intercepts the *x*-axis at a modulus value of about 190 GPa. If the

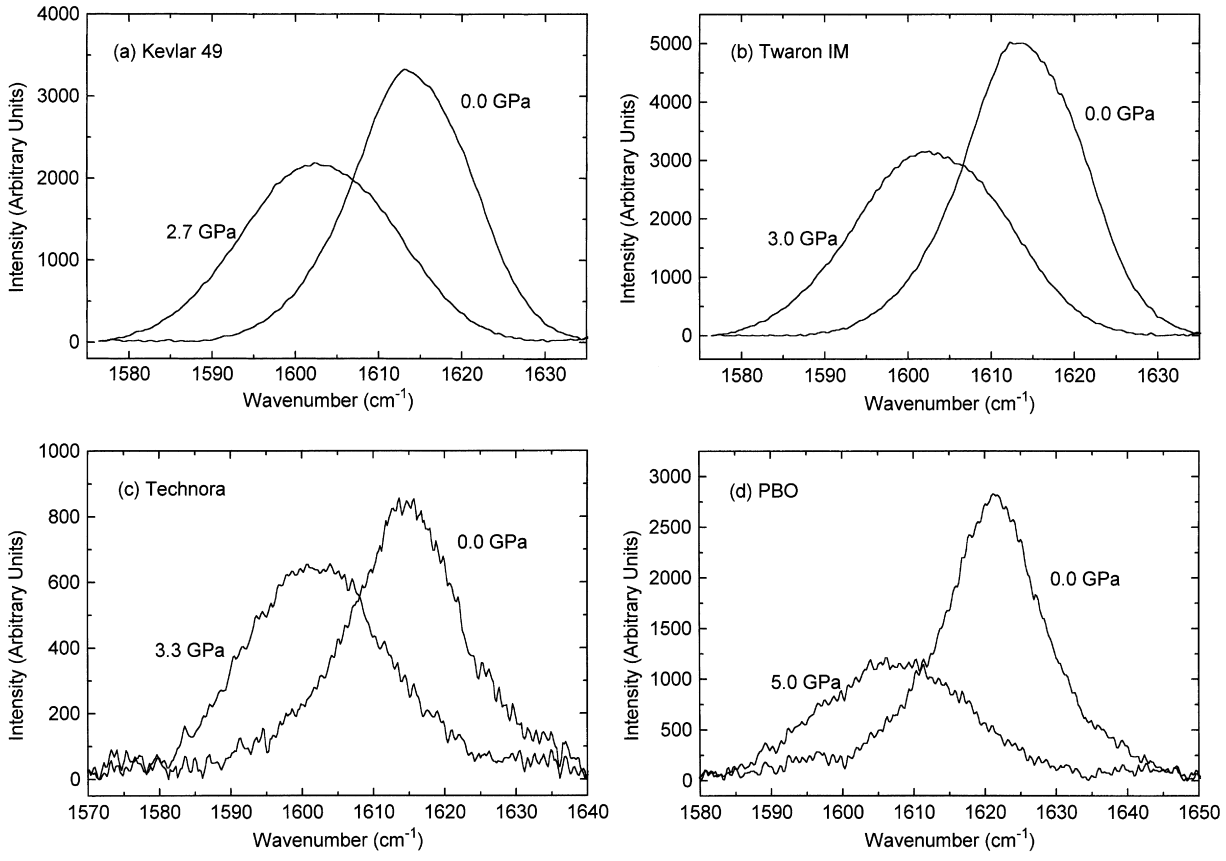

Fig. 8. Raman band shifts at (a) 1610 cm^{-1} for Kevlar, (b) 1610 cm^{-1} for Twaron, (c) 1614 cm^{-1} for Technora and 1621 cm^{-1} for PBO, subjected to a tensile stress.

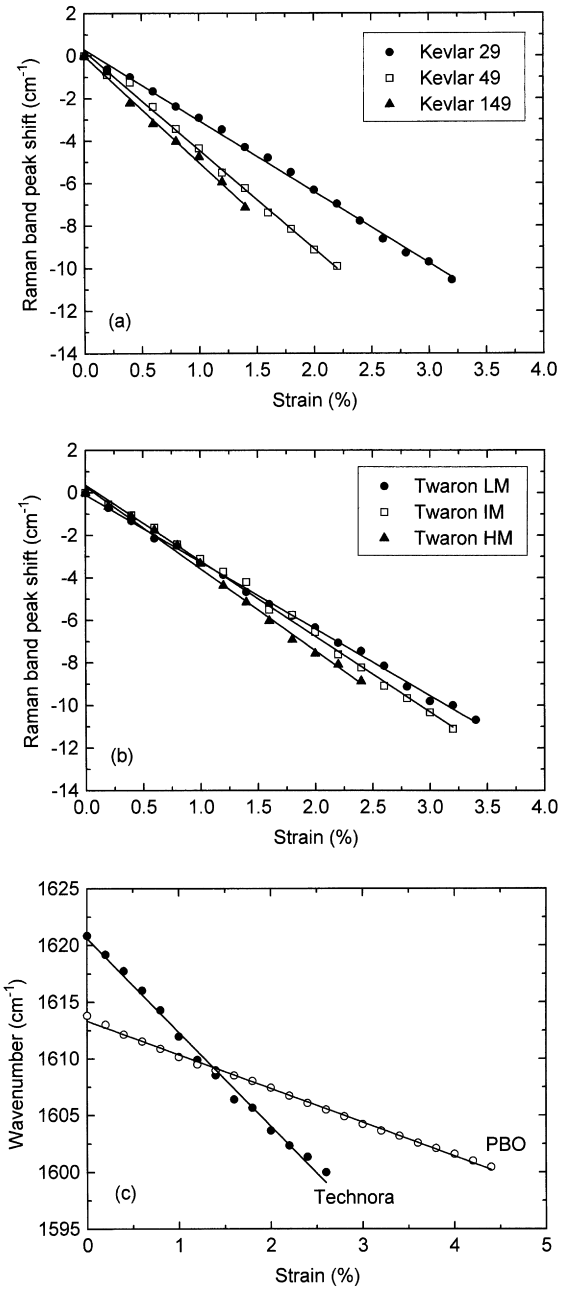

Fig. 9. Raman band peak shifts at (a) 1610 cm^{-1} for Kevlar, (b) 1610 cm^{-1} for Twaron, (c) 1614 cm^{-1} for Technora and 1621 cm^{-1} for PBO fibres, subjected to tensile strain.

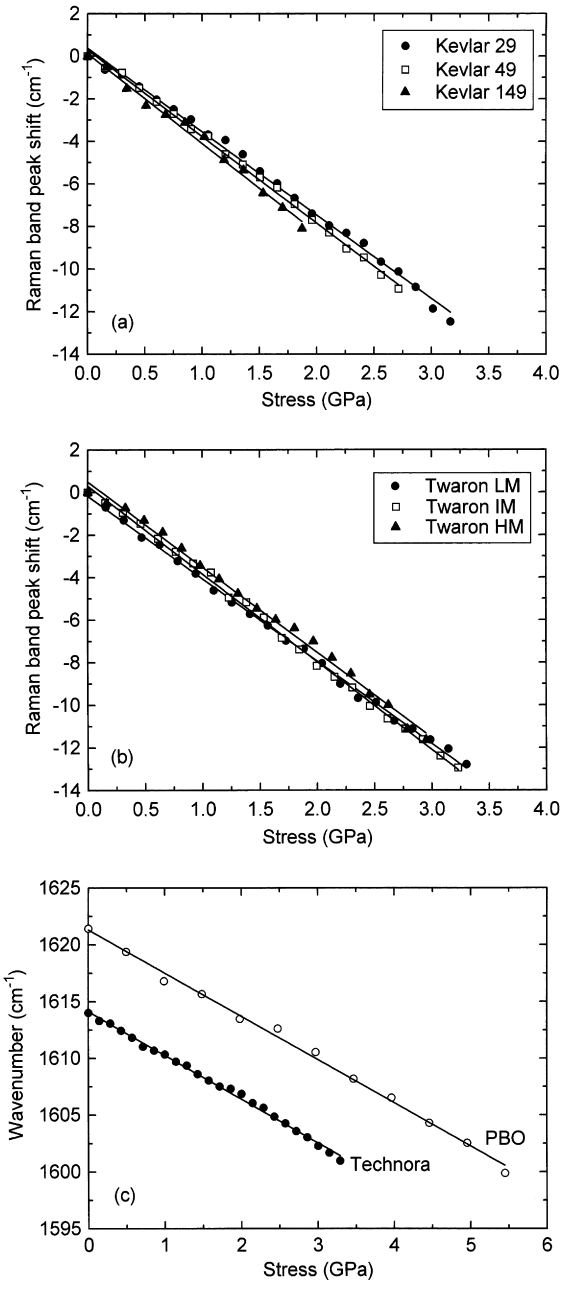

Fig. 10. Raman band peak shifts at (a) 1610 cm^{-1} for Kevlar, (b) 1610 cm^{-1} for Twaron, (c) 1614 cm^{-1} for Technora and 1621 cm^{-1} for PBO fibres, subjected to a tensile stress.

broadening is due to an uneven distribution of molecular stress then it should fall to zero for a perfect PPTA crystal and this value of modulus should correspond to that of a PPTA crystal. The value of 190 GPa is in good agreement with the X-ray measured crystallite modulus of 153–200 GPa [29–31].

The shifts of the *p*-phenylene ring vibration Raman bands with stress are shown in Fig. 8*c* and *d* for the Technora and PBO fibres, respectively. It can be seen that the Raman bands shift to lower wavenumber and broaden during tensile deformation. The Raman bands for these two fibres are again symmetric for both the undeformed and deformed fibres, i.e. the *SI* values [10] equal to 1. Hence, again the Lorentzian curve fitting procedure was employed to analyse all of the Raman spectra. The shift of the 1614 cm^{-1} band for the Technora fibre and of the 1621 cm^{-1} band for PBO with strain are approximately linear up to fracture, as shown in Fig. 9*c*. The PBO fibre gives the highest value of strain-induced band shift factor of all the high-performance polymer fibres studied in this work (Table 4), i.e. −8.1 cm^{-1}/%, and the Technora fibre has the lowest value, i.e. −2.9 cm^{-1}/%. The strain-induced band shift

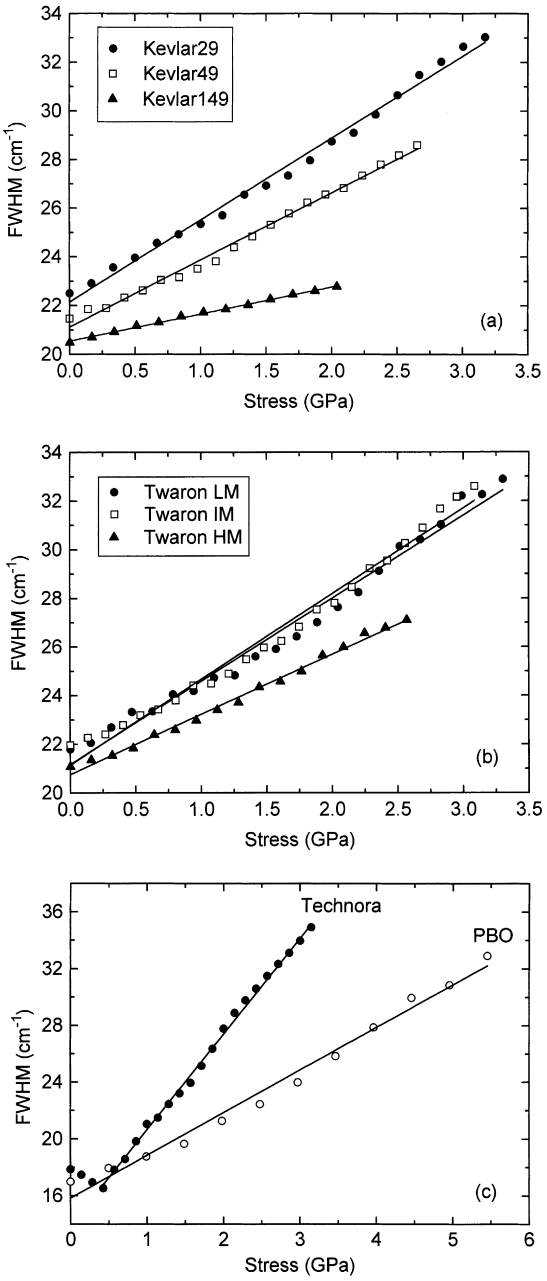

Fig. 11. The variation of FWHM of (a) the 1610 cm^{-1} Raman band for Kevlar, (b) the 1610 cm^{-1} Raman band for Twaron, (c) the 1614 cm^{-1} Raman band for Technora and the 1621 cm^{-1} Raman band for PBO, subjected to a tensile stress.

factor of $-8.1\ cm^{-1}$/% for the heat-treated PBO fibre is close to the value of $-7.9\ cm^{-1}$/% reported by Young *et al.* [7] and Ang [17] for PBO fibres from a different source.

Fig. 10*c* shows the dependence of the peak positions of the 1614 cm^{-1} Raman band for the Technora fibre and the 1621 cm^{-1} Raman band for the PBO fibre upon stress. Again, the Raman band shift is proportional to the stress and data for both fibres fall on lines of identical slope, i.e. approximately $-4.0\ cm^{-1}$/GPa (Table 4). This figure is the same as the value observed for the both the Kevlar and Twaron fibres described above. It implies that the molecular

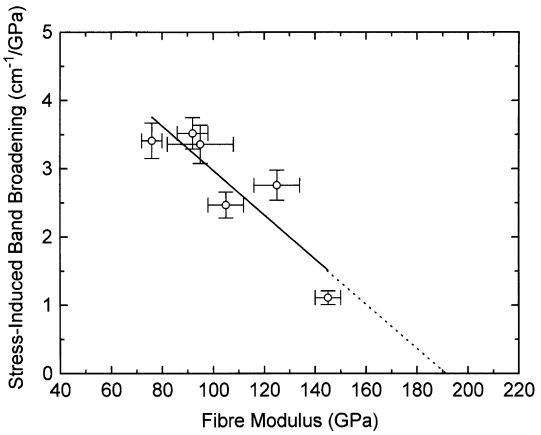

Fig. 12. Variation of stress-induced band broadening of the 1610 cm^{-1} Raman band as a function of fibre modulus for Kevlar and Twaron aramid fibres.

deformation process in all these different types of fibres are similar, even though the fibres have different chemical structures and processing histories.

Technora and PBO fibres exhibit somewhat different band broadening behaviour, as shown in Fig. 11*c*. The value of FWHM first decreases for the Technora fibre from 18 to 16.5 cm^{-1} up to the application of 0.5 GPa stress, and the value of FWHM then increases linearly as a function of stress. The decrease of FWHM at low stress may be due to its distinctly different morphology from that of the other fibres [15] which results in rearrangement of the molecules or crystallites in the fibres in the early stages of deformation. The modulus also shows a first maximum at about 0.4 GPa (Fig. 5) which may be due to the same reason. This distinctly different morphology also yields a much higher value of the stress-induced band broadening factor (about 6.8 cm^{-1}/GPa) for stresses above 0.5 GPa. The value of FWHM for the PBO fibre nearly doubles from 17 to 33 cm^{-1}, but the stress-induced band broadening factor is only 2.1 cm^{-1}/GPa since PBO has the highest Young's modulus (192 GPa) among the high-performance polymer fibres investigated.

3.5. Comparison with PET fibres

It is of interest at this stage to compare the behaviour of the different types of fibres investigated with that of PET fibres studied earlier[28]. The chemical repeat unit for PET is given below:

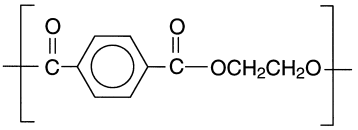

and it can be seen that it also contains a *p*-phenylene group. There is a Raman band at 1616 cm^{-1} assigned to the vibrational mode 8a of the *p*-phenylene ring [22,27,28] and

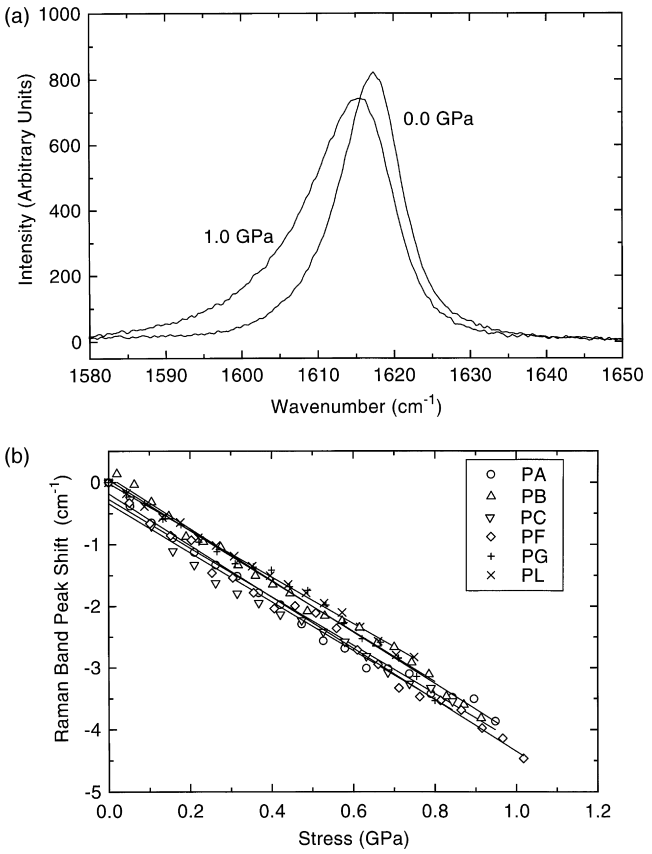

Fig. 13. Stress-induced shifts of the 1616 cm^{-1} Raman band for PET fibres. (a) Change in peak position for a stress of 1 GPa and (b) dependence of the peak position upon stress for a number of different fibres [28].

Fig. 13*a* shows the change in peak position and band shape of this band for a commercial Diolen® PET fibre [32] subjected to a stress of 1.0 GPa. It can be seen that the band moves to lower wavenumber and becomes more asymmetric [28]. This increased asymmetry is in marked contrast to the behaviour of the aramid, and PBO fibres described earlier in this present investigation where the bands remain symmetric under stress. It implies that there must be a number of over-stressed bonds in the deformed PET fibres [28].

Fig. 13*b* shows the dependence of the centre of gravity (to take into account the band asymmetry [28]) of the 1616 cm^{-1} Raman band upon stress for a number of PET fibres processed in different ways to give different mechanical properties. It is found that all of the data fall on lines with slopes of around -4.0 cm^{-1}/GPa, independent of the fibre structure [28]. This implies that the *p*-phenylene rings in the PET, aramid, and PBO fibres appear, during tensile deformation, to bear the same level of average molecular stress for a given level of macroscopic stress. The PET fibres have inferior mechanical properties to the other fibres due to the presence of amorphous regions and a poorer level of molecular orientation. The molecular deformation mechanisms of the different fibres, however, bear a remarkable similarity.

4. Modelling of deformation processes in the fibres

The four main findings in this work that need to be explained from a theoretical viewpoint are as follows:

- The rate of shift per unit stress of the ~1610 cm^{-1} Raman band is approximately -4.0 cm^{-1}/GPa for both PET fibres and all of the aromatic high-modulus fibres investigated in this present study.
- The Raman bands for the aramid and PBO fibres are symmetric and broaden under stress.
- The rate of band broadening in PPTA aramid fibres decreases with increasing modulus.
- The Raman bands for the PET are asymmetric and both broaden and become more asymmetric under stress.

Some of the above points have been addressed already but they are discussed in detail below in the context of models that have been developed to analyse the molecular deformation processes in high-performance fibres.

4.1. Uniform stress model for highly-oriented fibres

In Raman deformation studies, the *p*-phenylene ring vibration provides useful information concerning the state of molecular stress for a wide range of highly-oriented aromatic fibres and gives a unique insight into the mechanisms of molecular deformation. Wool *et al*. [33] investigated the effect of stress on infrared band frequencies and band asymmetry in highly-oriented isotactic polypropylene. The shifts appeared to be a linear function of stress and could be expressed by

$$\Delta\nu_\sigma = \nu(\sigma) - \nu(0) = \alpha_x\sigma \tag{3}$$

where $\Delta\nu_\sigma$ is the mechanically-induced band shift, α_x is the mechanically induced frequency shifting coefficient at constant temperature, and σ is the applied axial stress. The mechanically induced band shift factor α_x is a function of temperature, morphology, thermal history, and stress history[34]. It was assumed by Zhurkov and others [34] that α_x is a constant for each molecular vibrational mode. This has now been confirmed by the present study and it has been found to be approximately -4.0 cm^{-1}/GPa.

Hence the Raman band shift with the applied stress for the *p*-phenylene ring vibration 8a in the range of 1610–1620 cm^{-1} for the fibres can be described as follows:

$$\Delta\nu_\sigma = \alpha_x\sigma \tag{4}$$

where α_x represents the stress-induced band shift factor. The relationship observed in Eq. (4) can be differentiated and it becomes:

$$\mathrm{d}\Delta\nu_\sigma = \alpha_x\mathrm{d}\sigma \tag{5}$$

Then by dividing both terms by the axial strain differential,

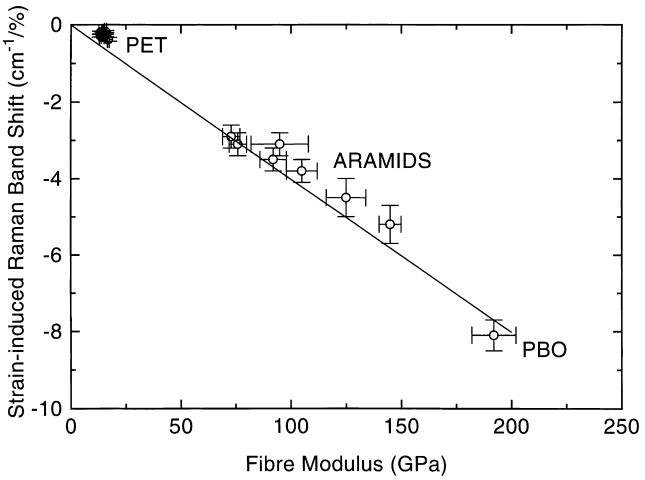

Fig. 14. Variation of strain-induced Raman band shift for the *p*-phenylene ring vibration with fibre Young's modulus for PET [30], Kevlar, Twaron, Technora and PBO fibres.

$d\epsilon$, we obtain:

$$\frac{d\Delta\nu_\sigma}{d\epsilon} = \alpha_x \frac{d\sigma}{d\epsilon} = \alpha_x E_f \tag{6}$$

where E_f is the Young's modulus of the fibre. The strain-induced shift of the *p*-phenylene ring vibration Raman band versus fibre modulus is plotted in Fig. 14 and it can be seen that the rate of shift appears to be proportional to the modulus for all of the fibres. The consequence of this is that the macroscopic Young's modulus of an aromatic polymer fibre can be determined if the value of the strain-induced shift of the *p*-phenylene ring vibration Raman band is measured.

4.2. Modified series aggregate model

There have been many of studies concerned with the effect of fibre microstructure upon the mechanical properties of polymer fibres and it is generally accepted that the behaviour can be explained in terms of an aggregate model [35]. A modified series aggregate model has been developed by Northolt and co-workers [36,37] to explain the non-linear elastic response of highly-oriented fibres. More recently Baltussen [38] has developed and refined this model in terms of his 'continuous chain model' to give a full explanation of the stress–strain behaviour of aramid, PET and cellulose fibres. In the modified series model it is assumed that the polymer fibre consists of parallel aligned fibrils containing a series of oblong crystallites with an orientation distribution around the fibre axis as shown schematically in Fig. 15*a*. Tensile deformation in polymer fibres takes place through the combined effect of [38]: (a) the elongation of the polymer chains; and (b) the shear deformation of small domains containing the chain segments.

This behaviour is shown schematically in Fig. 15*b* for an individual crystallite. For an infinitesimal deformation in highly-oriented fibres it is found that the fibre modulus is given by [20,38]

$$\frac{1}{E_f} = \frac{1}{e_c} + \frac{\langle \sin^2\Theta \rangle_E}{2g} \tag{7}$$

where e_c is the polymer chain modulus, g is the shear modulus and $\langle \sin^2\Theta \rangle_E$ is the strain orientation parameter of the chains defined by

$$\langle \sin^2\Theta \rangle_E = \frac{\langle \sin^2\Theta \cos\Theta \rangle}{\langle \cos\Theta \rangle} \tag{8}$$

In the determination of the stress–strain behaviour of polymer fibres it is necessary to use the theory of elasticity for finite deformations [38]. A major factor controlling non- linear deformation for polymer fibres will be the rotation of the domains causing a change in orientation of the chain segments from $\Theta \rightarrow \theta$ due to a tensile stress σ_f. In the case of highly-oriented fibres the strain in the chains, ϵ_c, can be approximated by σ_f/e_c and the overall fibre strain is given by[38]

$$\epsilon_f = \frac{\sigma_f}{e_c} + \frac{\langle \cos\theta \rangle - \langle \cos\Theta \rangle}{\langle \cos\Theta \rangle} \tag{9}$$

which means that the overall fibre strain is the sum of that due to the strain of the chain segments and the rotation strain, i.e.

$$\epsilon_f = \epsilon_{\text{stretch}} + \epsilon_{\text{rotation}} \tag{10}$$

This equation is vital in the design of high-modulus fibres where it is essential that the amount of chain stretching is maximized and rotation kept to a minimum through a high degree of molecular alignment. Moreover it also explains the Raman band shifts being proportionally higher for higher-modulus fibres (Fig. 14) since the band shift is due only to chain stretching and not rotation.

Another prediction of the model is that the modulus of the fibres should increase with increasing strain as the crystallites rotate towards the tensile axis [20,38]. This is clearly the case for the aramid fibres as shown in Fig. 3. The modulus also increases with strain, at least initially, for the Technora and PBO fibres (Figs 5 and 6). However, at higher strains their modulus values peak (with two peaks for Technora). The difference in behaviour between the PBO fibres and the PPTA fibres may be because molecular slippage may occur at higher strains since there is no inter-chain hydrogen bonding in PBO. It is not so clear why the behaviour of the Technora is different from that of Kevlar and Twaron but it may be again due to molecular slippage. The inter-chain H-bonding may not be so efficient in the copolymer and the WAXS pattern in Fig. 1*c* shows less well-defined inter-chain ordering.

The Raman data provide evidence for this model since there is no asymmetric broadening to lower wavenumber for the *p*-phenylene ring vibration during tensile deformation for Kevlar, Twaron, Technora and PBO fibres. All Raman spectra shift to lower wavenumber due to the application of

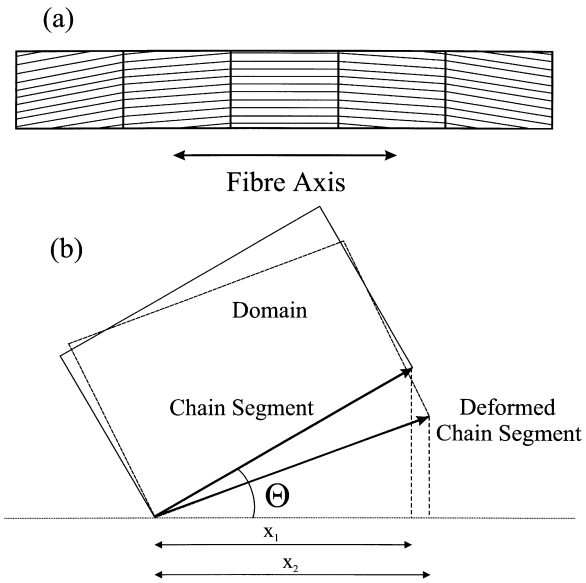

Fig. 15. Continuous chain model of Baltussen [35] for the deformation of polymer fibres. (a) Fibril containing crystallites with an orientation distribution and (b) deformation behaviour of an individual crystallite showing the elongation and rotation of a chain segment.

stress on these fibres. It was found that the Raman band shifts were a linear function of stress for the *p*-phenylene ring vibration for the Kevlar and Twaron fibres which gave an identical value of the stress-induced band shift of about $-4.0\ \mathrm{cm}^{-1}$/GPa, as obtained for the PET fibres [28]. Both Technora and PBO fibres also gave an identical value of about $-4.0\ \mathrm{cm}^{-1}$/GPa. Interestingly, the Technora and PBO fibres exhibit the similar deformation processes, i.e. controlled by a uniform stress, irrespective of their different chemical structure, physical morphology and microstructure. Nevertheless, even though the structures are different, it appears that the stress experienced by the *p*-phenylene ring groups is similar for the same macroscopic stress on the fibres.

5. Conclusions

Using Raman spectroscopy, it is found that a variety of high-performance aramid (including Kevlar, Twaron and Technora fibres) and PBO fibres undergo the same molecular deformation processes that can be explained by using a modified series model. The symmetric vibrational mode of the *p*-phenylene ring provides a useful Raman band to monitor the molecular deformation during tensile stretching of these fibres. The Raman band shift was also observed to be related to tensile stress rather than tensile strain for the high-performance polymer fibres. It was found that Raman band shift is proportional to the stress and lines for different fibres all have identical slope, i.e. about $-4.0\ \mathrm{cm}^{-1}$/GPa, which is the same as the value observed for PET fibres. This implies that the molecular deformation process in all of these different types of fibres are similar even though the fibres have different chemical structure and have been processed differently.

Acknowledgements

The fibres used in this work were kindly supplied by Akzo Nobel Research (Netherlands), Du Pont (USA), Teijin Ltd (Japan) and Toyobo Ltd (Japan). This work was supported by grants from the EPSRC and the Royal Society. One of the authors (RJY) is grateful to the Royal Society for support in the form of the Wolfson Research Professorship in Materials Science.

References

[1] Lemstra PJ, Kirschbaum R, Ohta T, Yasuda H. in *Developments in Oriented Polymers—2*, Chap. 2. Elsevier Applied Science, London, 1987.
[2] Yang HH. *Aromatic High-Strength Fibers*. Wiley-Interscience, New York, 1989.
[3] Young RJ. J Text Institute 1995;86:361.
[4] Galiotis C. Robinson IM, Young RJ, Smith BJE, Batchelder DN. Polymer Commun 1985;26:354.
[5] van der Zwaag S, Northolt MG, Young RJ, Robinson IM, Galiotis C, Batchelder DN. Polymer Commun 1987;28:276.
[6] Day RJ, Robinson IM, Zakikhani M, Young RJ. Polymer 1987;28:1833.
[7] Young RJ, Day RJ, Zakikhani M. J Mater Sci 1990;25:127.
[8] Andrews MC, Lu D, Young RJ. Polymer 1997;38:2379.
[9] Bower DI, Maddams WF. *The Vibrational Spectroscopy of Polymers*. Cambridge University Press, Cambridge, 1992.
[10] Suffolk BR, Gilpin RK. Anal Chem 1985;57:596.
[11] Northolt MG, van Aartsen JJ. J Appl Polym Sci Polym Lett Edn 1973;11:333.
[12] Northolt MG. Eur Polym J 1974;10:799.
[13] Tashiro K, Kobayashi M, Tadokoro H. Macromolecules 1977;10:413.
[14] Blackwell J, Cageao RA, Biswas A. Macromolecules 1990;23:2843.
[15] Cageao RA, Schneider A-I, Biswas A, Blackwell J. Macromolecules 1990;23:2843.
[16] Krause SJ, Haddock TB, Vezie DL, Lenhert PG, Hwang WF, Price GE, Helminiak TE, O'Brien JF, Adams WW. Polymer 1988;29:1354.
[17] Ang PP. Deformation micromechanics of high modulus polymer fibres and composites, Ph.D. Thesis, Victoria University of Manchester, 1991.
[18] Northolt MG, van Aartsen JJ. J Appl Polym Sci, Polym Symp 1977;58:283.
[19] Northolt MG. Polymer 1980;21:1199.
[20] Northolt MG, van der Hout R. Polymer 1985;26:310.
[21] Kitagawa T, Murase H, Yabuki K. J Polym Sci, Polym Phys 1998;36:39.
[22] Kim PK, Chang C, Hsu SL. Polymer 1986;27:34.
[23] Young RJ, Lu D, Day RJ. Polym Int 1991;24:71.
[24] Andrews MC, Young RJ. J Raman Spect 1993;24:539.
[25] Andrews MC, Day RJ, Hu X, Young RJ. Compos Sci Technol 1993;48:255.
[26] Andrews MC, Day RJ, Hu X, Young RJ. J Mater Sci Lett 1992;11:1344.
[27] Colthup NB, Wiberley SE, Daly LH. Introduction to Infrared and Raman Spectroscopy. Academic Press, London, 1975, p. 258.
[28] Yeh W-Y, Young RJ. J Macromol Sci Phys 1998;B37:83.

[29] Gaymans RG, Tijssen J, Harkama S, Bantjes H. Polymer 1976;17:517.
[30] Slustker LI, Utevskii LE, Yu Chereiskii Z, Perepelkin KE. J Polym Sci, Polym Symp 1977;58:339.
[31] Ii T, Tashiro K, Kobayashi M, Tadokoro H. Macromolecules 1987;20:347.
[32] van der Heuvel CJM, Heuvel HM, Fassen WA, Veurink J, Lucas LJ. J Appl Polym Sci 1993;49:925.
[33] Bretzlaff RS, Wool RP. Macromolecules 1983;16:1907.
[34] Zhurkov SN, Korsukov VI, Novak II. *Fracture 1979. Proceedings of the 2nd International Conference on Fracture*, p. 545.
[35] Ward IM. *Mechanical Properties of Solid Polymers*. Wiley, London, 1971.
[36] Northolt MG, van der Hout R. Polymer 1985;26:310.
[37] Northolt MG, Sikkema DJ. Adv Polym Sci 1990;98:119.
[38] Baltussen JJM. Tensile deformation of polymer fibres, Ph.D. Thesis, Technical University of Delft, 1996.